AN EXACT SOLUTION FOR INCORPORATING BOUNDARY CONTINUITY CONSTRAINTS IN SUBBAND ALL-POLE MODELLING

James R. Hopgood

Institute for Digital Communications,
School of Engineering and Electronics, University of Edinburgh
http://www.see.ed.ac.uk/~jhopgoo1
James.Hopgood@ed.ac.uk

Simon I. Hill

Signal Processing Laboratory,
Department of Engineering, University of Cambridge
http://www-sigproc.eng.cam.ac.uk/
sih22@eng.cam.ac.uk

ABSTRACT

Subband all-pole modelling is a flexible, scalable, and powerful approach for parsimoniously modelling rational transfer functions. Its advantage lies in its ability to model frequency bands independently of one another, thereby resulting in lower model orders in each subband and an overall reduction in the required number of parameters. To alleviate discontinuities in the spectrum at subband boundaries, it is necessary to increase slightly the computational complexity of the problem by incorporating continuity constraints. Previous solutions for implementing these constraints have been formulated for mathematical tractability and convenience; however, they are approximate and introduce modelling artifacts. This paper outlines an exact solution to the constrained modelling problem by using Lagrangian multipliers. The modelling results improve on the approximate formulations previously published.

1. INTRODUCTION

The modelling of complicated transfer functions, such as those encountered in acoustical signal processing, requires a highly flexible and scalable parametric model. The *full band all-pole model* is frequently used, but results in high model orders since it attempts to fit the entire frequency range simultaneously, even though it may fit some regions in the frequency space better than others. Full band all-pole modelling of acoustic impulse responses (AIRs) with reverberation times of $T_{60} \approx 0.5$ seconds typically require model orders in the range $50 \leq P \leq 500$ [1], or even higher; estimating this number of parameters requires a large computational load that can be unacceptable in computationally intensive algorithms such as blind dereverberation.

An intuitive rationale for why high-model orders result is as follows: consider a transfer function that is highly resonant in a low frequency band, and much less resonant in a higher band, as shown in Figure 1. Spencer [2] shows that this response can be accurately modelled by an all-pole model with 72 parameters. The low frequency band, upto $\approx$ 2kHz, is highly resonant, and can be modelled using ≈ 12 poles. These poles are near the unit circle, and the response due to each pole-pair quickly rolls-off at 40dB per decade. Consequently, a significant amount of 'effort' is needed to model the low-Q responses residing at high frequencies, since they need to counteract the roll-off effect of the low-frequency high-Q poles. Thus, when this response is modelled using a single all-pole filter, a large number of poles are needed. On the other hand, the *unconstrained subband all-pole model* does not face this problem since it fits different frequency bands independently, leading to a parsimonious approximation of the rational transfer functions and lower model orders. It is shown in [3] that the response in Figure 1, when using 3 subbands, can be modelled using just 51 parameters: almost a third fewer parameters. Subband linear prediction was first considered in [4] and developed in [3, 5–7].

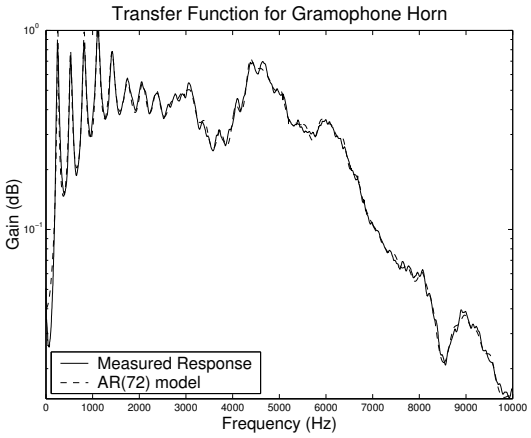

Fig. 1. The transfer function of an acoustic gramophone horn horn [2], and the corresponding AR model; Response, $0 \rightarrow 10$ kHz.

Complete decoupling of the subbands leads to discontinuities in the model's spectrum at the subband boundaries, introducing modelling artifacts. To circumvent this problem, continuity across subband boundaries much be enforced, as shown in [3]. However, the solution in [3], while being straightforward and computationally efficient to implement, is an unsatisfactory approximation. This paper outlines an exact solution to the constrained subband modelling problem using Lagrangian multipliers. The results are compared with the approximate formulation reported in [3].

Except where indicated, the set notation $\mathcal{G} = \{1, \ldots, G\} \subset \mathbb{Z}$ is used; *e.g.* $\mathcal{N}_i = \{1, \ldots, N_i\}$.

2. SIGNAL MODEL

When a system response is modelled as all-pole excited by white Gaussian noise (WGN), the random signal at the output, $x(t)$, is given by the autoregressive (AR) process:

$$x(t) = -\sum_{p=1}^{P} a(p)\, x(t-p) + \sigma\, e(t) \qquad (1)$$

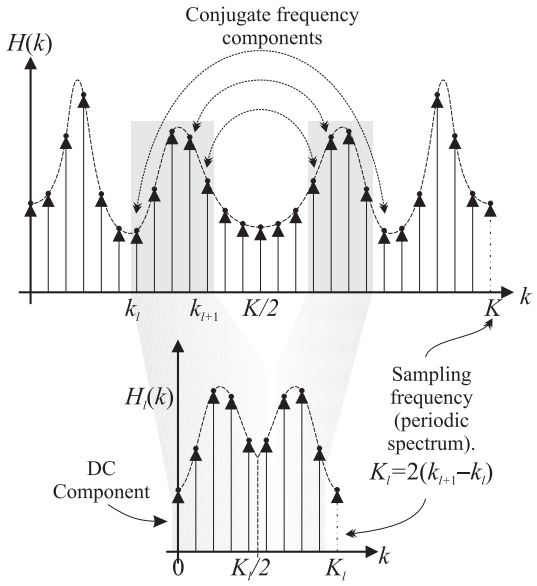

Fig. 2. Subband modelling and the indices mapping. The frequency bin nearest the half sampling frequency is $k_{\frac{f_s}{2}} = \lfloor \frac{T}{2} \rfloor$.

where $e(t)$ is unit variance WGN input excitation. The filter's transfer function is therefore:

$$H(k) = \frac{X(k)}{E(k)} = \frac{\sigma}{1 + \sum_{p=1}^{P} a(p)\, e^{-\frac{2j\pi kp}{T}}} \tag{2}$$

This is the *full-band all-pole model*. The *subband all-pole model* uses L subbands: in each subband, $x(t)$ is modelled by an all-pole spectrum in frequency bins $k \in \{k_\ell,\, \ldots,\, k_{\ell+1}-1\}$, where $\ell \in \mathcal{L}$ denotes the subband index, $K_\ell = 2(k_{\ell+1}-k_\ell) = T_\ell$ is the number of frequency components in the band, and $\{k_\ell,\, \ell \in \mathcal{L}\}$ are the subband boundaries; $k_0 \triangleq 0$ and $k_\ell \triangleq T$. The transfer function in a particular subband is obtained from (2) using the mapping [4]

$$k \rightarrow \frac{k-k_\ell}{K_\ell} = \frac{k-k_\ell}{2(k_{\ell+1}-k_\ell)}, \quad \text{for } k\,T \leq 2 \tag{3}$$

such that the transfer function of the subband model is:

$$H(k) = \sum_{\ell=0}^{L-1} \frac{\sigma_\ell \sqrt{\frac{K_\ell}{K}}\, \mathbb{I}_{\{k_\ell, k_{\ell+1}\}}(k)}{1 + \sum_{p=1}^{P_\ell} a_\ell(p)\, e^{-\frac{\pi\, j(k-k_\ell)p}{k_{\ell+1}-k_\ell}}} \tag{4}$$

where $\mathbf{a}_\ell = \{a_\ell(p),\, p \in \mathcal{P}_\ell\}$ and $\sigma_\ell \in \mathbb{R}^+$ denote model parameters in subband l, and the indicator function $\mathbb{I}_{\mathcal{A}}(a) = 1$ if $a \in \mathcal{A}$ and zero otherwise. The term $\sqrt{\frac{K_\ell}{K}}$ is required in equation (4) to ensure that the *energy* in the spectrum in conserved through the spectral mapping defined in equation (3). The mapping procedure given by equation (3) is graphically shown in Figure 2.

2.1. Likelihood Function for AR Processes

Since the discrete Fourier transform (DFT) is an orthonormal transformation, the probability density function (pdf) of the DFT of a Gaussian random process is Gaussian [3]. Hence, if the vector of excitation samples given by $[\mathbf{e}]_t = e(t),\, t \in \mathcal{T}$ has pdf[1] $p_e(\mathbf{e}) = \mathcal{N}\left(\mathbf{e} \,\middle|\, \mathbf{0}_T,\, \mathbf{I}_T\right)$, then the vector of excitation spectral components, $\boldsymbol{\mathcal{E}} = \mathbf{W}_T\, \mathbf{e}$, where $\mathbf{W}_T$ is the DFT matrix, has pdf $p_E(\boldsymbol{\mathcal{E}}) \propto \mathcal{N}\left(\boldsymbol{\mathcal{E}} \,\middle|\, 0,\, \mathbf{I}_T\right)$ [3]. The spectral excitation, $\boldsymbol{\mathcal{E}}$, is divided into subbands, $\boldsymbol{\mathcal{E}} = [\,\boldsymbol{\mathcal{E}}_0,\, \ldots,\, \boldsymbol{\mathcal{E}}_{L-1}]^T$, where $[\boldsymbol{\mathcal{E}}_\ell]_k = E(k-k_\ell)$, $k \in \{k_\ell,\, \ldots,\, k_{\ell+1}-1\}$. Hence, it follows:

$$p_E(\boldsymbol{\mathcal{E}}) \propto \prod_{\ell=0}^{L-1} \mathcal{N}\left(\boldsymbol{\mathcal{E}}_\ell \,\middle|\, 0,\, \mathbf{I}_{T_\ell}\right) \tag{5a}$$

Assuming the number of spectral components in each subband is large, such that linear convolution can be approximated by circular convolution, it can easily be shown that when using the *subband all-pole model*, the subband spectral excitation can be written in the usual linear form [3]:

$$\sigma_\ell\, \boldsymbol{\mathcal{E}}_\ell = \boldsymbol{\mathcal{X}}_\ell + \mathbf{X}_\ell\, \mathbf{a}_\ell \tag{5b}$$

where $[\boldsymbol{\mathcal{X}}_\ell]_k = X(k-k_\ell)$, and $[\mathbf{X}_\ell]_{k,p} = e^{-\frac{\pi j(k-k_\ell)p}{k_{\ell+1}-k_\ell}} X(k-k_\ell)$. Using the probability transformation rule, the likelihood function is given by:

$$p(\,\boldsymbol{\mathcal{X}} \mid \boldsymbol{\theta},\, \boldsymbol{\phi}) \propto \prod_{\ell=0}^{L-1} \frac{1}{(2\pi\sigma_\ell^2)^{\frac{T_\ell}{2}}} \exp\left\{-\frac{\|\boldsymbol{\mathcal{X}}_\ell + \mathbf{X}_\ell\, \mathbf{a}_\ell\|^2}{2\sigma_\ell^2}\right\} \tag{6}$$

where $\|\cdot\|$ denotes the Euclidean norm, $\boldsymbol{\theta} = \{\mathbf{a}_\ell,\, \sigma_\ell^2,\, \ell \in \mathcal{L}\}$ are the model parameters, and $\boldsymbol{\phi}$ is a vector of parameters representing the positions of the subband boundaries and model orders. The maximum-likelihood estimate (MLE) follows straightforwardly from maximising (6), and gives the familiar solutions:

$$\begin{aligned} \hat{\mathbf{a}}_\ell &= -\left(\mathbf{X}_\ell^\dagger \mathbf{X}_\ell\right)^{-1} \Re\left\{\mathbf{X}_\ell^\dagger\, \boldsymbol{\mathcal{X}}_\ell\right\} \\ \hat{\sigma}_\ell^2 &= \frac{1}{T_\ell}\left[\boldsymbol{\mathcal{X}}_\ell^\dagger\, \boldsymbol{\mathcal{X}}_\ell + \Re\left\{\mathbf{X}_\ell^\dagger\, \boldsymbol{\mathcal{X}}_\ell\right\} \mathbf{a}_\ell\right] \end{aligned} \tag{7}$$

3. SUBBAND BOUNDARY CONSTRAINTS

Since the subbands are modelled independently, discontinuities arise at boundaries, but can be avoided by placing a constraint on the model parameters to ensure continuity. This constraint is derived from (4) as follows: if $k = k_{\ell+1}$ in subband $\ell+1$, then

$$H(k) = \frac{\sigma_{\ell+1}\sqrt{\frac{K_{\ell+1}}{K}}}{1 + \sum_{p=1}^{P_{\ell+1}} a_{\ell+1}(p)} \tag{8a}$$

Moreover, if $k = k_{\ell+1}$ in subband ℓ, then:

$$H(k) = \frac{\sigma_\ell \sqrt{\frac{K_\ell}{K}}}{1 + \sum_{p=1}^{P_\ell} (-1)^p\, a_\ell(p)} \tag{8b}$$

Equating these leads to the constraint:

$$\sum_{p=1}^{P_{\ell+1}} a_{\ell+1}(p) = \left(\frac{\hat{\sigma}_{\ell+1}}{\hat{\sigma}_\ell} - 1\right) + \frac{\hat{\sigma}_{\ell+1}}{\hat{\sigma}_\ell} \sum_{p=1}^{P_\ell} (-1)^p\, a_\ell(p) \tag{9}$$

where $\hat{\sigma}_\ell = \sigma_\ell \sqrt{K_\ell}$. Recall that the spectrum of the all-pole model has zero gradient at zero and half sampling frequencies; thus, (9) provides continuity in the function value and first derivative of $H(k)$, but not necessarily in higher derivatives.

[1] $\mathbf{I}_T \in \mathbb{R}^{T\times T}$ is the identity matrix, and $\mathbf{0}_T$ is the $T \times 1$ vector of 1s.

3.1. Approximate Solution

An approximate solution as presented in [3] involves writing one parameter in subband ℓ in terms of the other parameters in that subband, and the parameters in an adjacent subband which are assumed to be known. The details presented here are slightly different to those outlined in [3], in that the equations are presented in a more flexible manner, and the notation is consistent with the proposed approach in §3.2. Thus, writing equation (9) as:

$$\underbrace{\begin{bmatrix} a_{\ell+1}(1) \\ \vdots \\ a_{\ell+1}(P_{\ell+1}) \end{bmatrix}}_{\mathbf{a}_{\ell+1}} = \frac{\hat{\sigma}_{\ell+1}}{\hat{\sigma}_\ell} \left\{ \begin{bmatrix} \mathbf{0}_{P_\ell} \\ \mathbf{1}'^{T}_{P_\ell} \end{bmatrix} \begin{bmatrix} a_\ell(1) \\ \vdots \\ a_\ell(P_\ell) \end{bmatrix} + \begin{bmatrix} 0 \\ \vdots \\ 1 \end{bmatrix} \right\} + \begin{bmatrix} 0 \\ \vdots \\ -1 \end{bmatrix} + \begin{bmatrix} \mathbf{I}_{P_\ell} \\ -\mathbf{1}^{T}_{P_\ell} \end{bmatrix} \underbrace{\begin{bmatrix} a_{\ell+1}(1) \\ \vdots \\ a_{\ell+1}(P_\ell) \end{bmatrix}}_{\hat{\mathbf{a}}_{P_{\ell+1}}} \tag{10}$$

where $\mathbf{1}_P \in \mathbb{R}^P$ is the P length vector of 1s, and $\mathbf{1}'_P \in \mathbb{R}^P$ is P length the vector of alternating entries $-1, +1, \ldots$. Hence, (10) may be written in the form

$$\mathbf{a}_{\ell+1} = \mathbf{u}_\ell + \frac{\hat{\sigma}_{\ell+1}}{\hat{\sigma}_\ell} \{\mathbf{v}_\ell + \mathbf{B}_\ell \, \mathbf{a}_\ell\} + \mathbf{C}_{\ell+1} \, \hat{\mathbf{a}}_{\ell+1} \tag{11}$$

where $\hat{\mathbf{a}}_{\ell+1} \in \mathbb{R}^{P_{\ell+1}-1}$ is the new reduced parameter vector for subband $\ell+1$. Substituting into equation (5b), and rearranging *assuming* the parameters in the adjacent subband are *known* gives the all-pole linear-in-the-parameters expression:

$$\hat{\sigma}_\ell \, \boldsymbol{\mathcal{E}}_\ell = \hat{\boldsymbol{\mathcal{X}}}_\ell + \hat{\sigma}_\ell \, \hat{\boldsymbol{\mathcal{X}}}' + \hat{\mathbf{X}}_\ell \, \hat{\mathbf{a}}_\ell \tag{12}$$

The spectral excitation is a function of the parameters in adjacent subbands, and consequently, a full maximum-likelihood analysis should take this into account. Unsurprisingly, the resulting likelihood function is analytically intractable. Thus, an approximation is to calculate the subband parameters for the first subband assuming no continuity constraint, and then iterate through each of the subbands calculating the parameters in subband ℓ given the parameters in subband $\ell-1$ using the continuity constraint. Since equation (12) is linear in $\hat{\mathbf{a}}_\ell$, a MLE for this approximation follows relatively straightforwardly, and is detailed in [3].

Results for this approach are satisfactory from a modelling perspective and, as an example, the result when the response in Figure 1 is modelled using 10 subbands with continuity constraints is shown in Figure 3. The equalised response is smooth with no discontinuities. A penalty, however, is that the total number of required parameters is now 76, compared to 72 in the full band all-pole model, and 49 in the unconstrained subband all-pole model. Nevertheless, the individual subband model orders are small and so, overall, the computational load is reduced.

Still, despite the success of this formulation, this approach is unsatisfactory in that the implementation of the constraint is only for mathematical convenience. Why, for example, in equation (10) is parameter $a_{\ell+1}(P_{\ell+1})$ chosen for substitution, rather than any of the other parameters $\{a_{\ell+1}(1), \ldots, a_{\ell+1}(P_\ell)\}$? These conceptual difficulties can be alleviated by formulating the problem using Lagrangian multipliers, as shown in the next section.

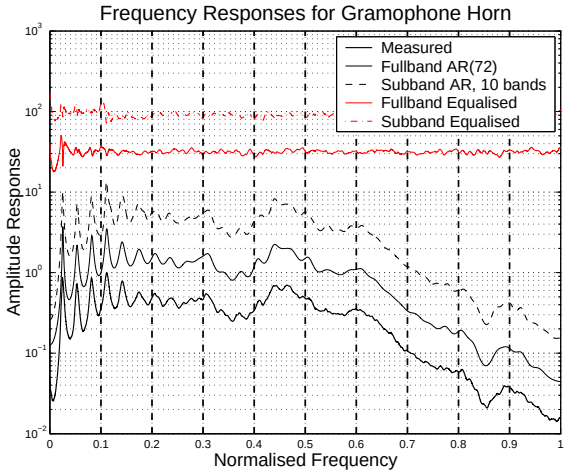

Fig. 3. Modelling the transfer function in Figure 1 by 10 subbands and a continuity constraint, using the implementation from §3.1.

3.2. Exact Solution using Lagrangian

3.2.1. Lagrangian Formulation

The negative log-likelihood function for all the subband parameters is obtained from (6), ignoring any normalising factors, as:

$$J_L(\boldsymbol{\theta}) = \sum_{\ell=0}^{L-1} \left\{ T_\ell \ln \sigma_\ell^2 + \frac{\|\boldsymbol{\mathcal{X}}_\ell + \mathbf{X}_\ell \, \mathbf{a}_\ell\|^2}{\sigma_\ell^2} \right\} \tag{13}$$

To obtain a MLE, whilst enforcing continuity, it is necessary to minimise $J_L(\boldsymbol{\theta})$ subject to the constraint in (9). If the k-th constraint is expressed in the form

$$C\left(\mathbf{a}_k, \, \mathbf{a}_{k+1}, \, \hat{\sigma}_k^2, \, \hat{\sigma}_{k+1}^2\right) = 0 \tag{14}$$

where $\hat{\sigma}_\ell^2 = T_\ell \sigma_\ell^2$ and $T_\ell \equiv K_\ell$, then combining (13) and (14) gives the Lagrangian cost function that needs to be minimised:

$$\mathcal{L}(\boldsymbol{\theta}) = J_L(\boldsymbol{\theta}) + \sum_{\ell=0}^{L-2} \lambda_\ell \, C\left(\mathbf{a}_k, \, \mathbf{a}_{k+1}, \, \hat{\sigma}_k^2, \, \hat{\sigma}_{k+1}^2\right) \tag{15}$$

There are many possibilities for how this constraint may be written, and two are discussed: the *linear*, and *quadratic* constraint.

3.2.2. Linear constraint

Equation (9) may be written as a linear constraint in terms of the $\mathbf{a}_k$'s, using the earlier definitions for $\mathbf{1}_\ell$ and $\mathbf{1}'_\ell$, as:

$$C\left(\mathbf{a}_k, \, \mathbf{a}_{k+1}, \, \hat{\sigma}_k^2, \, \hat{\sigma}_{k+1}^2\right) = \frac{1 + \mathbf{a}_{\ell+1}^T \mathbf{1}_{\ell+1}}{\sqrt{T_{\ell+1}}\sigma_{\ell+1}} - \frac{1 + \mathbf{a}_\ell^T \mathbf{1}'_\ell}{\sqrt{T_\ell}\sigma_\ell} = 0 \tag{16}$$

Substituting (16) into (15), taking derivatives, with respect to (w. r. t.) all the model parameters, σ_k and $\mathbf{a}_k$, and setting to zero in order to find a stationary point in the Lagrangian function gives:

$$\mathbf{a}_k = -\left(\mathbf{X}_k^\dagger \mathbf{X}_k\right)^{-1} \Re\{\mathbf{X}_k^\dagger \, \boldsymbol{\mathcal{X}}_k\} + \left(\mathbf{X}_k^\dagger \mathbf{X}_k\right)^{-1} \left\{ \frac{\lambda_k \, \sigma_k \mathbf{1}'_k}{2\sqrt{T_k}} - \frac{\lambda_{k-1} \, \sigma_k \mathbf{1}_k}{2\sqrt{T_k}} \right\} \tag{17a}$$

$$0 = 2T_k\sigma_k^2 - 2\left\|\boldsymbol{\mathcal{X}}_k + \mathbf{X}_k\,\mathbf{a}_k\right\|^2 + \frac{\sigma_k}{\sqrt{T_k}}\left\{\lambda_k\left[1+\mathbf{a}_k^T\mathbf{1}_k'\right] - \lambda_{k-1}\left[1+\mathbf{a}_k^T\mathbf{1}_k\right]\right\} \tag{17b}$$

$$\sigma_{k+1} = \sigma_k\sqrt{\frac{T_k}{T_{k+1}}}\frac{1+\mathbf{a}_{k+1}^T\mathbf{1}_{k+1}}{1+\mathbf{a}_k^T\mathbf{1}_k'} \tag{17c}$$

where, by definition, $\lambda_{-1} = \lambda_{L-1} = 0$. Note that equation (17c) is just a rearrangement of the continuity constraint in equation (16).

Finding a solution to the set of nonlinear simultaneous equations in (17) is not straightforward and, evidently, analytical solutions are not forthcoming. An iterative solution might be considered, especially since (17a) can be written as the sum of a least-squares estimate (LSE), and a component due to the constraints, thereby providing the LSE as a natural starting point. Unfortunately, the authors found that a direct implementation of an iterative solution failed, with parameter values diverging. A further problem with this formulation is the inter-dependency of the model parameters, thereby preventing any simplification of these equations. Consequently, a quadratic constraint is considered instead.

3.2.3. Quadratic constraint

The quadratic equivalent of the constraint in (9) is simply:

$$\frac{\left[1+\mathbf{a}_{\ell+1}^T\mathbf{1}_{\ell+1}\right]^2}{T_{\ell+1}\sigma_{\ell+1}^2} - \frac{\left[1+\mathbf{a}_\ell^T\mathbf{1}_\ell'\right]^2}{T_\ell\sigma_\ell^2} = 0 \tag{18}$$

Hence, the Lagrangian in equation (15) becomes:

$$\mathcal{L} = \sum_{\ell=0}^{L-1}\left\{T_\ell\ln\sigma_\ell^2 + \frac{\left\|\boldsymbol{\mathcal{X}}_\ell + \mathbf{X}_\ell\,\mathbf{a}_\ell\right\|^2}{\sigma_\ell^2}\right\} + \sum_{\ell=0}^{L-2}\lambda_\ell\left\{\frac{\left[1+\mathbf{a}_{\ell+1}^T\mathbf{1}_{\ell+1}\right]^2}{T_{\ell+1}\sigma_{\ell+1}^2} - \frac{\left[1+\mathbf{a}_\ell^T\mathbf{1}_\ell'\right]^2}{T_\ell\sigma_\ell^2}\right\} \tag{19}$$

where $\lambda_{-1} = \lambda_{L-1} = 0$. Similar to the linear constraint case, to minimise this expression, set the derivatives w. r. t. all the model parameters and Lagrange multipliers to zero. The derivatives are:

$$\nabla_{\mathbf{a}_k}\mathcal{L} = 2\frac{\Re\{\mathbf{X}_k^\dagger\,\boldsymbol{\mathcal{X}}_k\} + \mathbf{X}_k^\dagger\,\mathbf{X}_k\,\mathbf{a}_k}{\sigma_k^2} + \frac{2\lambda_{k-1}}{T_k\sigma_k^2}\left[\mathbf{1}_k\mathbf{1}_k^T\mathbf{a}_k + \mathbf{1}_k\right] - \frac{2\lambda_k}{T_k\sigma_k^2}\left[\mathbf{1}_k'\mathbf{1}_k'^T\mathbf{a}_k + \mathbf{1}_k'\right] \tag{20a}$$

$$\frac{\partial}{\partial\sigma_k^2}\mathcal{L} = \frac{T_k}{\sigma_k^2} - \frac{\left\|\boldsymbol{\mathcal{X}}_k + \mathbf{X}_k\,\mathbf{a}_k\right\|^2}{\sigma_k^4} - \frac{\lambda_{k-1}}{T_k\sigma_k^4}\left[1+\mathbf{a}_k^T\mathbf{1}_k\right]^2 + \frac{\lambda_k}{T_k\sigma_k^4}\left[1+\mathbf{a}_k^T\mathbf{1}_k'\right]^2 \tag{20b}$$

$$\frac{\partial}{\partial\lambda_k}\mathcal{L} = \frac{\left[1+\mathbf{a}_{k+1}^T\mathbf{1}_{k+1}\right]^2}{T_{k+1}\sigma_{k+1}^2} - \frac{\left[1+\mathbf{a}_k^T\mathbf{1}_k'\right]^2}{T_k\sigma_k^2} \tag{20c}$$

Setting equation (20a) to zero, and rearranging, it follows that:

$$\mathbf{Y}_k\,\mathbf{a}_k = -\mathbf{y}_k \tag{21}$$

where the real-valued matrix $\mathbf{Y}_k$ and vector $\mathbf{y}_k$ are given by:

$$\mathbf{Y}_k = \mathbf{X}_k^\dagger\,\mathbf{X}_k - \frac{\lambda_k}{T_k}\mathbf{1}_k'\mathbf{1}_k'^T + \frac{\lambda_{k-1}}{T_k}\mathbf{1}_k\mathbf{1}_k^T$$
$$\mathbf{y}_k = \Re\{\mathbf{X}_k^\dagger\,\boldsymbol{\mathcal{X}}_k\} - \frac{\lambda_k}{T_k}\mathbf{1}_k' + \frac{\lambda_{k-1}}{T_k}\mathbf{1}_k \tag{22}$$

Equation (20b) may be written as:

$$\sigma_k^2 - \frac{1}{T_k}\left\|\boldsymbol{\mathcal{X}}_k + \mathbf{X}_k\,\mathbf{a}_k\right\|^2 = \frac{\lambda_{k-1}}{T_k^2}\left[1+\mathbf{a}_k^T\mathbf{1}_k\right]^2 - \frac{\lambda_k}{T_k^2}\left[1+\mathbf{a}_k^T\mathbf{1}_k'\right]^2 \tag{23}$$

Note that equation (20c), when set to zero, yields the continuity constraint in (18). To solve the constrained optimisation problem, the exercise now falls to solving equations (18) and (21), and (23). Although these equations are difficult to solve analytically, there are some interesting features of these equations to note: given the observed data in the matrices $\mathbf{X}_k$ and vectors $\boldsymbol{\mathcal{X}}_k$, then

1. equation (21) is a function of the Lagrange multipliers only,
2. given all the subband AR parameters and the first subband variance, all the other variances can be evaluated using a rearrangement of equation (18):

$$\sigma_{k+1}^2 = \frac{T_k}{T_{k+1}}\sigma_k^2\left[\frac{1+\mathbf{a}_{k+1}^T\mathbf{1}_{k+1}}{1+\mathbf{a}_k^T\mathbf{1}_k'}\right]^2 \tag{24}$$

3. Given the subband AR parameters, and using equation (24), equation (23) may be written as L linear equations in L unknowns consisting of $\{\lambda_k\}_0^{L-2}$ and σ_0^2.

3.2.4. Minimising Lagrangian for Quadratic constraint

Attempts to solve equations (18) and (21), and (23) by an iterative recursive technique failed to yield convergent solutions. Further work is continuing to find efficient techniques to minimise the Lagrangian in equation (19), for example by investigating whether convexity properties are met by the function. Presently, however, the results in this paper are found by a straightforward minimisation of the cost function in (19), by utilising the relationships in equations (18) and (21). By substituting (18) and (21) into (19), the Lagrangian is now a function of the first subband variance, σ_0^2 and the Lagrange multipliers, $\{\lambda_k\}_0^{L-2}$: $\mathcal{L} = \mathcal{L}\left(\sigma_0^2,\,\{\lambda_k\}_0^{L-2}\right)$. The complete algorithm is summarised in Algorithm 1. Note the solution of equation (21) in step 14 is efficiently implemented by:

1. precomputing the matrix $\mathbf{X}_k^\dagger\,\mathbf{X}_k$ and the vector $\Re\{\mathbf{X}_k^\dagger\,\boldsymbol{\mathcal{X}}_k\}$ in equation (22),
2. finding $\mathbf{Y}_k^{-1}$ using the matrix inversion lemma

$$\left(\mathbf{A}+\lambda\mathbf{u}\mathbf{u}^T\right)^{-1} = \mathbf{A}^{-1} - \lambda\frac{\mathbf{A}^{-1}\mathbf{u}\mathbf{u}^T\mathbf{A}^{-1}}{1+\lambda\mathbf{u}^T\mathbf{A}^{-1}\mathbf{u}}$$

twice to deal with the last two terms in equation (22). As a result, it is possible to show that equation (21) may also be written as the sum of the LSE solution, and an additional *correction term*, similar to the expression in (17a).

The L parameters for the function LAGRANGECOSTFUNCTION in Algorithm 1 are the first subband variance, and the Lagrange multipliers. Thus, the dimensionality of the search space is equal to the number of subbands, and therefore is *relatively* low.

The minimisation in step 6 of the algorithm is performed using the Nelder-Mead Simplex method as implemented in MATLAB.[2]

[2]When using the Nelder-Mead Simplex method in a high-dimensional parameter space, the optimisation routine should always be restarted at a point where the algorithm claims to have found a minimum; this is to ensure that the algorithm is not fooled by local minima, or any other anomalies that might influence the convergence criteria [8]. Similarly, it is common to have multiple starting positions, checking the minimum function value is always found.

Algorithm 1 Constrained subband modelling algorithm

1: **procedure** LAGRANGEOPIMISATION($\{x(t)\}$, $\{k_\ell\}_{\ell=1}^{L-1}$)
2: Calculate spectral components, $X(k)$, from observed data, $x(t)$: $x(t) \overset{\text{DFT}}{\rightleftharpoons} X(k)$
3: Given the subband boundaries, $\{k_\ell\}$, estimate model orders for each subband, P_ℓ, assuming an *unconstrained* AR model, using for example, Akaike's information criterion.
4: Evaluate LSE for subband AR parameters, and excitation variance, $\sigma^2_{LSE,0}$, for the first subband by using (7) for $\ell = 0$.
5: Set initial conditions for subband variance $\sigma_0^2 = \sigma^2_{LSE,0}$ and Lagrange multipliers, $\lambda_k = 0$, $k \in \{0, \ldots, L-2\}$
6: **repeat**
7: Evaluate $\mathcal{L} =$ LAGRANGECOSTFUNCTION(σ_0^2, $\{\lambda_k\}_{k=0}^{L-2}$)
8: Update parameter estimates for σ_0^2 and λ_k.
9: **until** $\mathcal{L}$ is the global minimum of equation (19).
10: Determine subband parameters from (21) and (24) for these optimal values of σ_0^2, $\{\lambda_k\}_{k=0}^{L-2}$.
11: **end procedure**

12: **function** LAGRANGECOSTFUNCTION(σ_0^2, $\{\lambda_k\}_{k=0}^{L-2}$)
13: **for all** $k \in \{0, \ldots, L-1\}$ **do**
14: solve equation (21) for $\mathbf{a}_k$.
15: **end for**
16: **for all** $k \in \{0, \ldots, L-2\}$ **do**
17: solve equation (24) for σ^2_{k+1}.
18: **end for**
19: Evaluate equation (19) as a function of σ_0^2 and $\{\lambda_k\}_{k=0}^{L-2}$.
20: **end function**

This method simply crawls downhill in a straightforward fashion, making no assumption about the cost function in (19) [8]. Although this approach is slow, it is reasonably robust, and while further work is continuing to find a more efficient optimisation technique, the purpose of the present paper is to demonstrate the modelling ability of the constrained subband modelling approach.

3.2.5. *Model Order Selection*

The subband *model orders*, *changepoint* locations, and *number of subbands* must be chosen. Here, the number of subbands is chosen with the boundaries set uniformally distributed across the full frequency range, or in the case of any a few subbands, by manually choosing the boundaries away from high-Q resonances. Since data is being fitted by an AR model, each subband model order is selected using Akaike's B-Information criterion (BIC). Currently, however, the computational effort involved in the optimisation of step 6 of Algorithm 1 prevents model order selection being performed in the constrained modelling case. As a suboptimal solution, the model-orders are determined in the *unconstrained case*, as determined by the solutions of equation (7), using the BIC.

3.2.6. *Investigating Properties of Lagrangian Cost Function*

It is interesting to consider the cost function in equation (19) in the two-band case since it is easy to plot and therefore to gain some insight into its properties. The gramophone horn in Figure 1 is modelled, and (19) is plotted as a function of σ_0^2 and λ_0 in Figure 4. The resulting model response is shown in Figure 5, along with the actual system response, and the response obtained in the

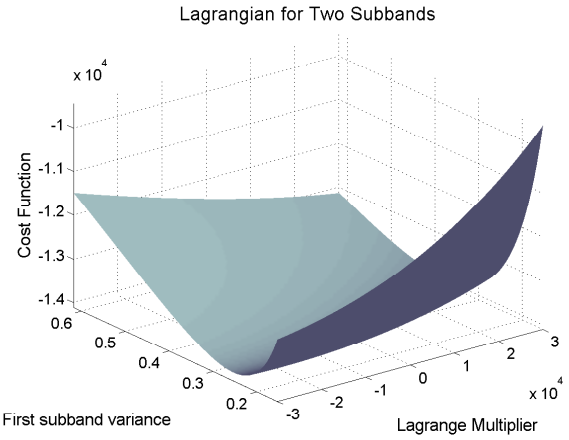

Fig. 4. Cost function of (19) for the two band case as a function of the first subband variance, σ_0^2, and the Lagrange multiplier λ_0.

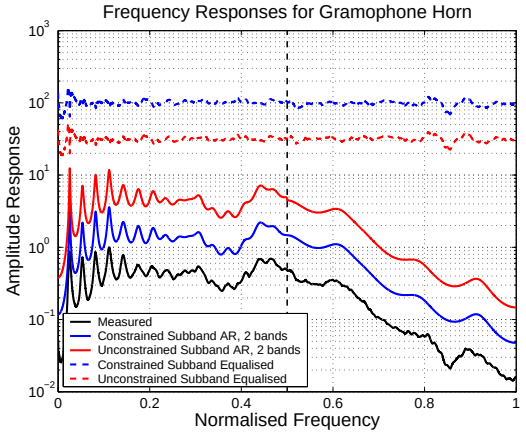

Fig. 5. Responses shown for two-subbands in the unconstrained and constrained cases. An offset has been included between curves to improve clarity. The equalised responses are also shown, and should be flat when modelling the actual response accurately.

unconstrained case. The model orders are $\{P_\ell\}_0^1 = \{37, 10\}$, so the total number of parameters is 25 fewer than in the fullband case. Although the difference between the unconstrained and constrained case is minor, on inspection the constrained case gives a slightly smoother response at the subband boundary. The effect of discontinuities are more pronounced when more subband boundaries are considered. The number of data points used is 2^{14}.

3.3. Experimental Results

To demonstrate the advantage of the constrained over the unconstrained subband modelling methods, the response in Figure 1 is modelled using 10 subbands, with the results shown in Figure 6. Discontinuities can clearly be seen in the *unconstrained case*, with a significantly smoother result in the *constrained case*. A couple of subbands are under-modelled, but this is an issue with the model-order selection procedure, not the constraint, since the undermodelling appears in both cases. The model orders are $\{P_\ell\}_0^9 = \{11, 8, 1, 2, 2, 2, 3, 1, 4, 2\}$, giving a total of 36 parameters,

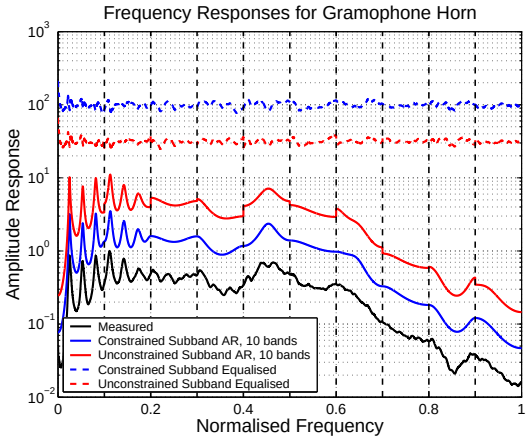

Fig. 6. Responses shown for 10-subbands in the unconstrained and constrained cases. See Figure 5 for plotting information.

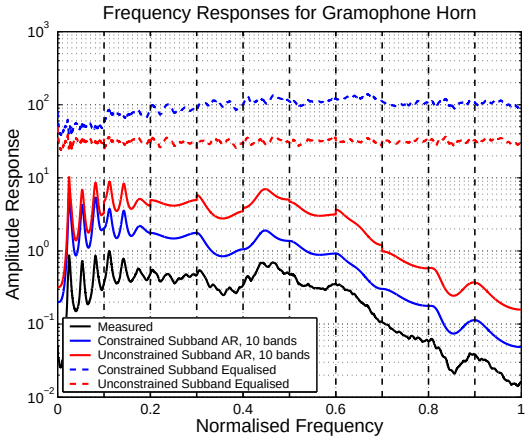

Fig. 7. Responses shown for 10-subbands in the unconstrained and gain-adjusted cases. See Figure 5 for plotting information.

Algorithm 2 Gain Adjust Continuity Constraint

1: **procedure** GAINADJUSTCONTINUITY($\{x(t)\}$, $\{k_\ell\}_{\ell=1}^{L-1}$)
2: Execute steps 2 to 3 of Algorithm 1.
3: Evaluate LSEs for all subbands using equation (7).
4: **for all** $k \in \{0, \ldots, L-2\}$ **do**
5: Adjust gains by solving equation (24) for σ_{k+1}^2.
6: **end for**
7: **end procedure**

half the 72 in the fullband case. The optimisation in step 6 of Algorithm 1 is very inefficient and, in this example, typically takes ~ 5000 function evaluations to converge. This is unacceptable in computational intensive algorithms. Proposals for overcoming this include considering equation (19) as a pdf, and using stochastic optimisation methods by considering the Lagrangian constraints as a prior, and the Lagrange multipliers as hyperparameters. These hyperparameters can then be sampled along with the other subband parameters. As the gradients of (19) are also known, other deterministic optimisation algorithms might also be appropriate.

Comparing the results of the Lagrangian constraint in Figure 6 with the approximate solution in §3.1, as shown in Figure 3, it is seen that the results are improved. The approximate solution is computationally less intensive, but also gives less robust results.

3.4. Gain-adjusted case

It is interesting to consider a dramatic simplification of the constrained optimisation discussed in §3.2.3 by using Algorithm 2. In this procedure, the AR parameters are estimated using the unconstrained model, but the subband variances are adjusted by solving (24) given the gain in an adjacent subband. The results are shown in Figure 7. The equalised response has a high-pass trend due to the accumulation of gain errors. This is likely to be unacceptable in many applications; however, since this simple approach is computationally very cheap, it may be useful in some circumstances.

4. CONCLUSIONS

The primary innovative result of this work is to extend the results presented in [3, 7] by formulating an exact solution to the problem of incorporating boundary continuity constraints in subband all-pole modelling. Without these constraints, subband all-pole modelling introduces distortion in the modelled response, as shown in [7], since each subband is decoupled from the others, thereby inducing discontinuities at the subband boundaries. Although continuity constraints have previously been described in [3], the solution was unsatisfactory in that it was an approximation made for mathematical and computational convenience. This paper outlines a formal approach to constrained optimisation using Lagrange multipliers, and it is shown that the modelling results outperform the approximate method, while giving a more satisfactory theoretical solution. Further work is needed to improve the computational efficiency of the method which, in the current implementation, is quite high. However, it is expected that stochastic optimisation methods may help, and consequently it should be possible to frame the approach in a natural Bayesian formulation.

5. REFERENCES

[1] J. N. Mourjopoulos and M. A. Paraskevas, "Pole and zero modeling of room transfer functions," *JSV*, vol. 146, no. 2, pp. 281 – 302, Apr. 1991.

[2] P. S. Spencer, *System Identification with Application to the Restoration of Archived Gramophone Recordings*, Ph. D. Thesis, University of Cambridge, UK, June 1990.

[3] J. R. Hopgood and P. J. W. Rayner, "Bayesian formulation of subband autoregressive modelling with boundary continuity constraints," in *Proc. IEEE ICASSP*, Hong Kong, Apr. 2003.

[4] J. Makhoul, "Spectral analysis of speech by linear prediction," *IEEE Trans. Audio and Electro.*, vol. AU-21, no. 3, pp. 140–148, June 1973.

[5] S. L. Tan and T. R. Fischer, "Linear prediction of subband signals," *IEEE J. Sel. Areas Comms.*, vol. 12, no. 9, pp. 1576–1583, Dec. 1994.

[6] S. Rao and W. A. Pearlman, "Analysis of linear prediction, coding, and spectral estimation from subbands," *IEEE Trans. Information Theory*, vol. 42, no. 4, pp. 1160–1178, July 1996.

[7] J. R. Hopgood and P. J. W. Rayner, "A probabilistic framework for subband autoregressive models applied to room acoustics," in *11th Proc. IEEE SSP*, Aug. 2001, pp. 492 – 494.

[8] W. H. Press, S. A. Teukolsky, W. T. Vetterling, and B. P. Flannery, *Numerical Recipes in C*, Cambridge University Press, 2nd edition, 1992.